Computers in Biology and Medicine 104 (2019) 205–214

Contents lists available at ScienceDirect

Computers in Biology and Medicine

journal homepage: www.elsevier.com/locate/compbiomed

Finite element analysis for fatigue behaviour of a self-expanding Nitinol peripheral stent under physiological biomechanical conditions

Long Lei[a,b], Xiaozhi Qi[a], Shibo Li[a,*], Yuanyuan Yang[a,**], Ying Hu[a], Bing Li[b], Shijia Zhao[a], Yanfang Zhang[c]

[a] Shenzhen Key Laboratory of Minimally Invasive Surgical Robotics and System, Shenzhen Institutes of Advanced Technology, Chinese Academy of Sciences, Shenzhen 518055, China
[b] Harbin Institute of Technology (Shenzhen), Shenzhen 518055, China
[c] Department of Interventional Radiology, Shenzhen People's Hospital, Shenzhen 518055, China

ARTICLE INFO

Keywords:
Peripheral artery disease
Finite element analysis
Nitinol stent
Fatigue fracture
Physiological deformation

ABSTRACT

Self-expanding Nitinol stents are increasingly used to treat femoropopliteal artery (FPA) occlusions, but the risk of stent fatigue failure exists due to complex artery deformation during daily activities. Finite element analysis (FEA) has been widely applied to study the stent fatigue behaviours, but physiological deformation and atherosclerotic plaque were not considered simultaneously in previous studies. In this work, to show the necessity and feasibility of considering both factors in evaluation of the stent fatigue behaviours, a comprehensive FEA framework considering both factors is established, and an easy loading method for the complex boundary condition is proposed. Four comparative simulations are successfully conducted, and the stent fatigue behaviours are analysed based on the distributions and maximum values of the self-defined mean and alternating strains. Results show that both the physiological deformation and atherosclerotic plaque significantly contribute to the stent fatigue life. The case with the complex boundary condition and atherosclerotic plaque is the most critical of the four cases, and the minimum safety factor is 0.62. In conclusion, it is necessary to consider both physiological deformation and atherosclerotic plaque in the evaluation of stent fatigue behaviours, and ignoring any of them would lead to overestimation of the stent fatigue life. The work in this paper offers a solid foundation for accurate evaluation of the stent fatigue lifetime in patient-specific surgery plans via FEA.

1. Introduction

Peripheral artery disease (PAD) is common among elderly people, and in 2015, PAD affected approximately 155 million people worldwide, among which 52500 patients died [1,2]. Lower limb artery disease, especially involving the superficial femoral artery (SFA) and popliteal artery (PA), is the most common PAD. This disease often results in discomfort, pain and other serious problems, such as intermittent claudication, heart disease, and stroke, when walking is involved. PAD is mainly caused by atherosclerosis, which induces vascular stenosis or occlusion and further causes a shortage of oxygen in maintenance of normal metabolism of the lower limb due to the reduction of blood flow.

Self-expanding Nitinol stents are increasingly popular in treatment of PAD, especially FPA stenosis. In daily activities, FPA undergoes large and complex deformations, such as cyclically axial compression, twisting and bending, in addition to the effect of blood pressure [3]. Despite its pseudo-elasticity [4], the Nitinol stent implanted in FPA still poses the potential risk of fatigue fracture. According to the review by Rits et al. [5], the risk range for reported stent fracture in SFA is 2–65%. The fractured stent might injure the vascular wall, thus resulting in re-occlusion of the artery and the requirement of additional treatments. Therefore, it is necessary to analyse the mechanical behaviours of the stent implanted in the diseased FPA to evaluate its fracture risk.

Some experimental studies of the fatigue fracture of the FPA stent have been conducted using in-house equipment [6–8] or commercial equipment [9]. These tests simplified the actual physiological environment and did not consider the anatomical characteristics of the actual diseased artery. Additionally, *in vitro* tests can supply the stent fatigue fracture result in a specific physiological environment but

* Corresponding author.
** Corresponding author.
E-mail addresses: long.lei@siat.ac.cn (L. Lei), xz.qi@siat.ac.cn (X. Qi), sb.li@siat.ac.cn (S. Li), yy.yang1@siat.ac.cn (Y. Yang), ying.hu@siat.ac.cn (Y. Hu), libing.sgs@hit.edu.cn (B. Li), sj.zhao1@siat.ac.cn (S. Zhao), szjieru0755@126.com (Y. Zhang).

https://doi.org/10.1016/j.compbiomed.2018.11.019
Received 31 July 2018; Received in revised form 25 November 2018; Accepted 25 November 2018

cannot produce the stress field and strain field in the stent.

Recently, FEA has been widely applied in analysis of the interaction between the stent and the surroundings because it can produce the stress and strain field information necessary to obtain a better understanding of the stent behaviour in the diseased artery. Early and Kelly [10] built a stent-artery coupling model to analyse the influence of axial bending and compression respectively on the risk of stent fatigue fracture. The results indicated that both bending and compression play a role in stent fracture, and the main factor depends on the implantation position within the arterial tree. However, in their studies, the artery was modelled as a tube with equal diameter and atherosclerotic plaque was ignored. Using FEA, The Laboratory of Biological Structure Mechanics (Politecnico di Milano, Italy) performed a great number of studies on the risk of stent fatigue [11–16]. Among these studies, Meoli et al. [12,14] analysed the fatigue behaviour of the Nitinol stent subjected to cyclic axial compression and bending in the fully-expanded and deployed configurations respectively. The results showed that it is necessary to consider the stent-artery interaction, and stent-to-vessel oversizing cannot be ignored in stent fatigue life analysis. Dordoni et al. [11] evaluated the influence of atherosclerotic plaque on stent fatigue resistance by defining three stenotic artery models with differing plaque sharpness and number of stenosis, periodic axial compression and bending were applied in their research. The results indicated that plaque plays an important role in the fatigue life prediction of the stent and should not be neglected. The drawback of this approach is that the single deformation boundary condition of axial compression or bending is applied to the stent, rather than the physiological deformation that the stent implanted in FPA undergoes. In addition, Harvey [17] constructed a FEA model of an actual artery generated from CT angiography to study the fatigue performance of the stent subjected to pulsatile and articulation loads, disregarding the plaque. Ghriallais and Bruzzi [18] investigated the effect of stent length and location on the deformation characteristics of the stented SFA using an anatomically accurate model of the leg, including necessary bones, muscles, and artery, during bending of the knee. The weakness of this approach is that the stented SFA model is obtained by simply increasing the local SFA stiffness, and it cannot be used in fatigue life analysis of the stent.

Based on the above discussion, the physiological deformation and atherosclerotic plaque were not considered simultaneously in the previous simulation analyses. In other words, the fatigue behaviours of the stent implanted into the stenotic artery subjected to physiological deformation remain unclear. To gain further insight into these points, in this work, a more comprehensive FEA model considering atherosclerotic plaque and physiological deformation is proposed, and four comparative simulations are conducted. Finally, the stent fatigue behaviours in different cases are quantitatively and qualitatively analysed based on the simulation results.

2. Methods

2.1. Geometry

A model of the diseased artery consisting of a straight artery with a single layer and a plaque is developed as shown in Fig. 1. The straight artery has a thickness of 0.7 mm, which is one tenth of its inner diameter (d_v) [19], to consider a stent-to-vessel oversizing ratio of 1.14. No statistical data on plaque shape are currently available. Generally, the plaque is considered to be uniform in the circumferential direction, and the thickness (t) is modelled according to the modified Hicks-Henne function [11,20,21] as follows

$$t = t_b + \left(\frac{d_v}{2}R_s - t_b\right)\sin\left(\frac{x}{L_P}\pi\right)^{\frac{1}{2}}, \quad 0 < x < L_P \tag{1}$$

where t_b is the base thickness of the plaque, L_P is the plaque length and R_s is the stenosis rate.

In this work, the length of the whole artery is 45 mm, and the values of t_b, L_P and R_s are respectively 0.5 mm, 28 mm and 50%.

A 3D geometrical model of the Nitinol peripheral stent is obtained from a commercial E•LUMINEXX ZVL08060 stent (Bard, USA), which is a cylindrical metal mesh tube produced in the fully expanded configuration and then crimped onto a catheter. The stent has a segmental repeating pattern, and its geometry when partially released from the sheath is shown in Fig. 2.

The modelling strategy for stent geometry can be summarized in three main steps (Fig. 3): Step 1: the DICOM images of the middle portion of the stent in the fully expanded configuration are acquired using μCT100 (SCANCO, Switzerland) with a resolution of 0.01 mm; Step 2: 3D reconstruction is performed to generate the virtual 3D model of the partially scanned stent (Fig. 3a) with the aid of Mimics (Materialise, Belgium), and the model dimensions are measured; Step 3: after the acquisition of model dimensions, the 2D sketch of two V-strut crowns (Fig. 3b) is drawn, extruded in the radial direction, arrayed in the axial direction, and modified for both ends (Fig. 3c). The stent model (Fig. 3d) is eventually built with ToroidalBend using Creo Parametric 3.0 (PTC, America). The model has an external diameter of 8 mm, a length of 25 mm, a strut width of 0.15 mm, and a strut thickness of 0.24 mm.

2.2. Material properties

The non-linear material properties of both the artery and plaque are described as a hyperelastic isotropic constitutive model using the third-order reduced polynomial strain energy density function reported in Eq. (2):

$$U = \sum_{i=1}^{3} C_i (I_1 - 3)^i \tag{2}$$

where C_i are material coefficients, and I_1 is the first strain invariant of the Cauchy-Green deformation tensor.

The material coefficients of the artery [22] are listed in Table 1. For the atherosclerotic plaque, a perfect plasticity model is used to represent inelasticity and damage [10,23,24], and the actual rupture stress is considered as the yield stress [23]. Cunnane et al. [25] performed FEA of diseased femoral artery revascularization based on the material data from atherosclerotic femoral artery tissue and aortic tissue, and the result shows that large differences between the two situations. Due to the large discrepancies, it is suggested that an

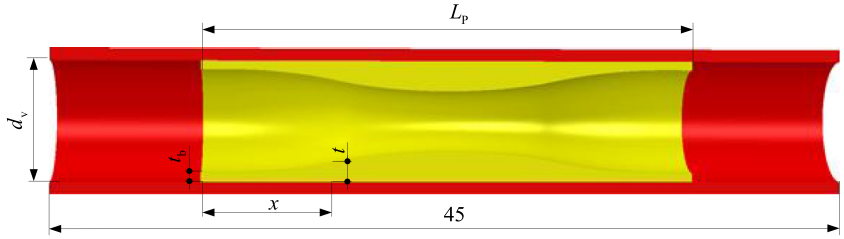

Fig. 1. Sectional view of the stenotic artery model.

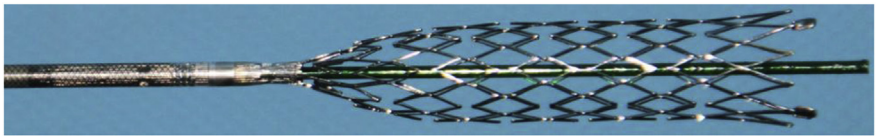

Fig. 2. E•LUMINEXX® stent partially released from the sheath.

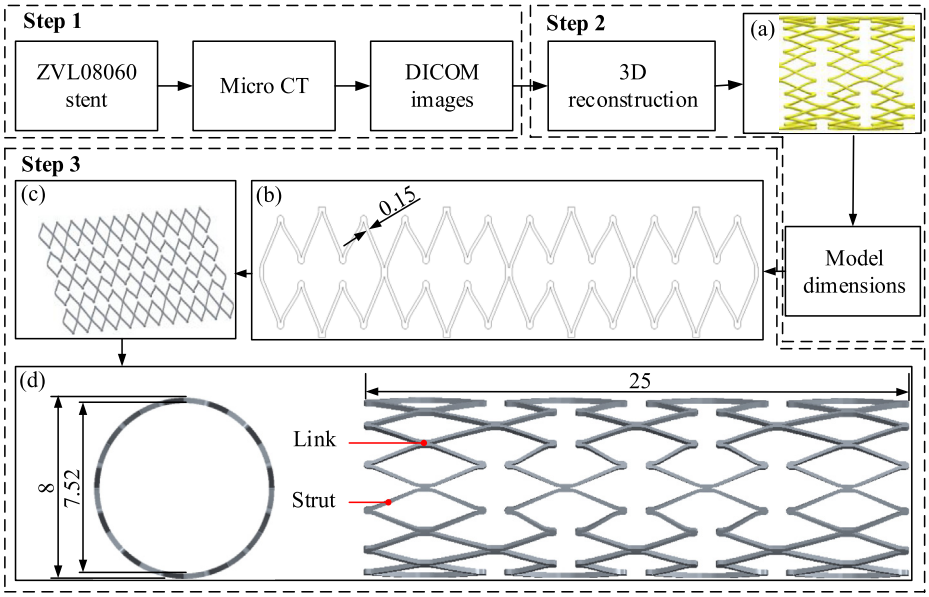

Fig. 3. Three-step modelling strategy for the stent geometry: (a) virtual 3D model generated from DICOM images; (b) 2D sketch of two V-strut crowns; (c) stent model obtained from 2D sketch after it is extruded in the radial direction, arrayed in the axial direction, and modified for both ends; (d) final stent model.

Table 1
Material coefficients of the artery and plaque.

Material	C_1(MPa)	C_2(MPa)	C_3(MPa)
Artery	1.05E-02	1.94E-02	1.10E-02
Plaque	4.62E-02	−1.47E-02	4.95E-03

Table 2
Material parameters of the Nitinol stent.

Parameters	Description	Values
E_A, E_M	Austenite and martensite Young's modulus	51100 MPa
ν	Austenite and martensite Poisson's ratio	0.3
ε_L	Transformation strain	0.04962
σ^S_{AM}	Start of transformation (loading)	416 MPa
σ^E_{AM}	End of transformation (loading)	442 MPa
σ^S_{MA}	Start of transformation (unloading)	185 MPa
σ^E_{MA}	End of transformation (unloading)	104 MPa
${}^C\sigma^S_{AM}$	Start of transformation in compression (loading)	611 MPa

appropriate plaque material should be adopted to simulate the interaction between the stent and the diseased femoral artery to obtain more accurate numerical results. Thus, the material coefficients of the heavily calcified femoral plaque tissue (Table 1) are applied, and a yield point of 0.16 MPa is defined in this work. More intuitively, the material characteristics of the artery and plaque are plotted in Fig. 4a.

The pseudo-elastic material behaviour of the Nitinol stent (Fig. 4b)

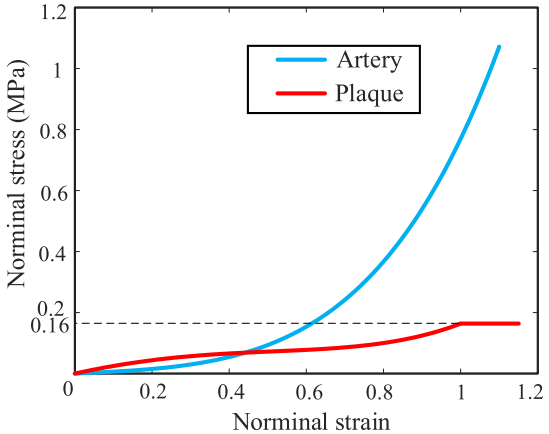

(a) Hyperelastic behaviours of the artery and plaque

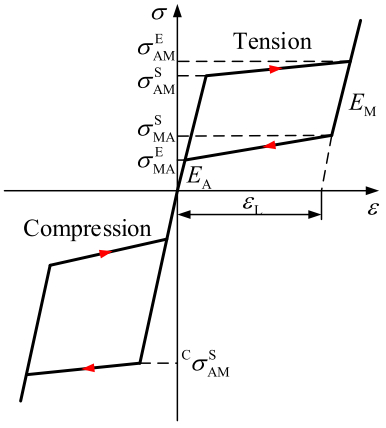

(b) Pseudo-elastic behaviour of Nitinol stent

Fig. 4. Material characteristics of the artery, plaque and Nitinol stent.

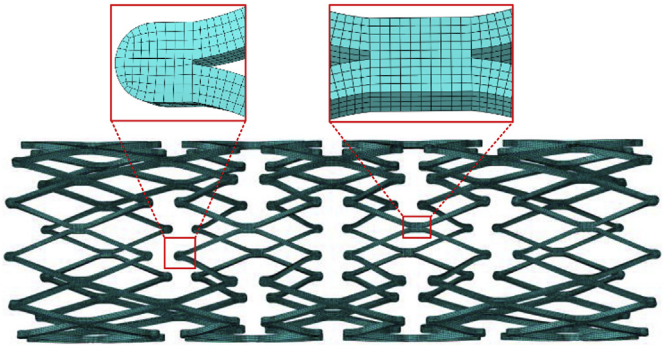

Fig. 5. Mesh of the stent model.

is described using the super elasticity model implemented by the user material subroutine (VUMAT) [26], and the model parameters [12] are listed in Table 2. During the loading-unloading process, direct and inverse material phase transformations between austenite and martensite take place and show a hysteretic cycle. Additionally, the material responses differ in tension and compression.

2.3. Modelling

The whole model consists of three instances, namely, the stenotic artery (partition into the artery and plaque cell), the stent, and the sheath used for crimping and expansion of the stent. Both the stent and stenotic artery models are meshed with incompatible 8-node linear brick elements (C3D8I). The sheath is modelled as a shell and discretized with reduced 4-node doubly curved shell elements with enhanced hourglass control and finite membrane strains (S4R). The stent is meshed more finely than the other instances, and a ratio of 0.25 is chosen for the element size between the stent and the stenotic model according to sensitivity analysis. The stent strut is discretized with four elements in both the width and thickness directions to avoid stress discontinuity, and the meshed stent model is shown in Fig. 5.

The simulation of the stenting procedure is completed in ABAQUS 2017/Explicit (Dassault Systèmes Simulia Corp., USA) due to the high nonlinearity including all material nonlinearity, geometric nonlinearity, and complex contact. The whole process can be simplified into six analysis steps: stent crimping, pre-stretching of the stenotic artery, free expansion of the stent, stent-driven stenotic artery expansion, and loading and unloading of the boundary conditions. All steps are solved as a displacement-driven contact problem, and the details are described as follows.

The stenotic artery, stent, and sheath are placed coaxially, and the

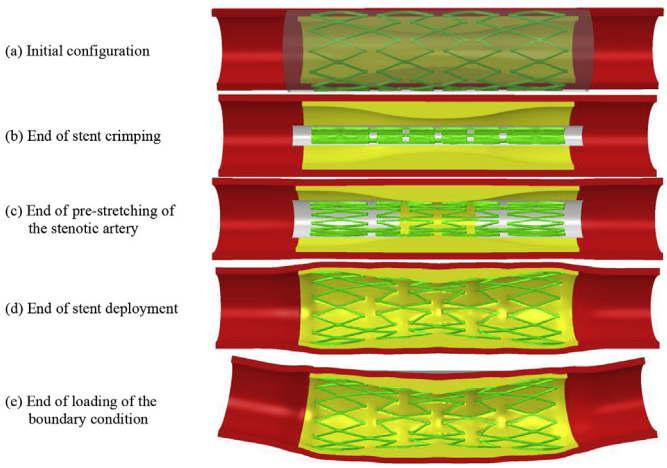

Fig. 6. Five typical simulation states during the stenting procedure.

whole model is axially symmetrical in the initial configuration (Fig. 6a). The inner diameter of the sheath is slightly smaller than the external diameter of the stent, with consideration of a small initial interference to prevent uncertain rigid body motion of the stent during stent crimping. A surface-to-surface contact pair between the inner surface of the sheath and the outer surface of the stent is established using the penalty contact method, and a tangential penalty friction coefficient of 0.2 is applied [10]. A negative radial displacement is imposed on all nodes of the sheath to crimp the stent to an external diameter of 2 mm (Fig. 6b), at which moment a considerable amount of strain energy is stored in the stent for the subsequent self-expansion. In addition, a frictionless self-contact is defined with the penalty contact method for the outer surface of the stent to avoid self-penetration, and the contact exists during the whole simulation. Pre-stretching of the stenotic artery is conducted to ensure the stability of the whole model when axially compressed, and the stent expands by gradually increasing the radial dimension of the sheath until the stent contacts the plaque (Fig. 6c). The surface-to-surface pair between the outer surface of the stent and the inner surface of the plaque is created. The positive radial displacement is continuously applied to the sheath, and the stent gradually expands the stenotic artery until the static equilibrium is reached at the same time (Fig. 6d). The contact between the sheath and the stent is deactivated, and the sheath no longer works in the subsequent analyses. Finally, the deformation boundary conditions are loaded (Fig. 6e) and unloaded successively to obtain the stent response subjected to the physiological load.

In addition, the same simulation analyses are also performed on a model without the atherosclerotic plaque.

2.4. Boundary conditions

Many available quantitative studies on SFA (stented and bare) deformation due to daily leg movement are available from cadavers and patients. Generally, the movement models consist of walking and sitting/stair climbing, corresponding respectively to 70°/20° and 90°/90° knee/hip bend angles [27–29]. In this work, the complex boundary condition including axial compression, bending and twisting is considered and loaded on the artery model, and the loading schematic is shown in Fig. 7.

As shown in Fig. 7, two reference points (RP1 and RP2) are created as control points to control the degrees of freedom of the nodes on the constraint surfaces (marked in purple) with the aid of kinematic coupling. The relative radial translation between the control point and the nodes of the constraint surface is not constrained considering the radial deformation of the stenotic artery model. The centreline of the deformed artery is assumed as a circular arch when the bending boundary condition is applied, and the centrelines of the stenotic artery in the initial and the deformed configurations are marked in blue and red, respectively. Additionally, α is the rotation angle around the T-axis, ΔL is the unilateral axial translation value, and θ is the unilateral rotation angle around the Z-axis. In the customized cylindrical coordinate system, α and ΔL are calculated as follows

$$\alpha = \frac{l}{2r} = \frac{(1 - R_c)L}{2r} \tag{3}$$

$$\Delta L = \frac{L}{2} - r \sin \alpha \tag{4}$$

where R_c is the axial compression rate, r is the radius of curvature, L and l are respectively the length of plaque in the initial and the deformed configurations.

A previous review [30] based on 12 relevant articles shows that the artery deformation decreases significantly when the stent is implanted, and the deformation during sitting is larger than during walking. The mean data from all articles for the proximal and middle superficial femoral artery (pSFA and mSFA) deformation during walking are adopted

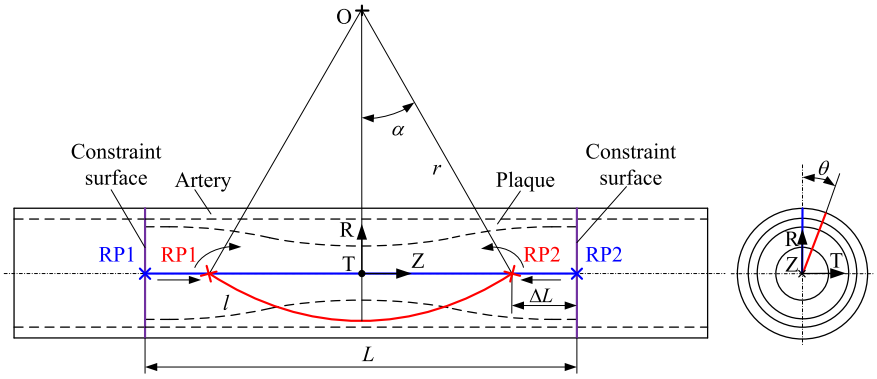

Fig. 7. Loading schematic of the complex boundary condition. The centrelines of the plaque in the initial and deformed configurations are marked in blue and red, respectively.

in this work, i.e., the values of R_c and r are respectively 4.0% and 72.1 mm, and an axial twisting of 0.21°/mm is considered. The pre-stretching ratio of 4.0% is also applied for the stenotic artery to restore its original length after compression [11].

To ensure that the simulation is quasi-static and efficient at the same time, the appropriate loading rate for each step should be used. In fact, the quasi-static analysis is achieved by taking at least 10 times the lowest-order mode period as the loading time for the deformation body. The stenotic artery has a far larger fundamental frequency than the stent when the true density values are defined. To meet the requirement of the quasi-static analysis simultaneously, the density of the stenotic artery is scaled down to a fundamental frequency approximately equal to that of the stent. Finally, the fundamental frequencies are 673.42 Hz for the stent and 486.12 Hz for the stenotic artery according to the frequency extraction analysis in ABAQUS/Standard, and the corresponding vibration modes are shown in Fig. 8. The step time periods for loading and unloading of the deformation boundary conditions are both 0.01 s in the specific simulation environment.

In addition, smooth step amplitude is applied to avoid fluctuation, and suitable additional damping is added to simulate the energy-absorbing characteristic of the actual system.

2.5. Fatigue criterion

Three methods are commonly used to assess the fatigue behaviour of the Nitinol: stress-life analysis, strain-life analysis and damage-tolerant analysis [31]. For strain-life analysis, some studies evaluated the Nitinol fatigue behaviours by using the first principal strains of the mean and alternating strain tensors as the mean strain and alternating strain [11,12,14], which proved appropriate for axial compression and bending conditions [15]. The von Mises equivalent mean and alternating strain are also used but are still questionable [17]. In this work, the same approach as in Ref. [11] is adopted for comparative purpose. A Python script is used to extract the logarithmic strain tensors at the end of the loading and unloading steps for each Gauss point, followed by calculation of the mean strain tensor ($\boldsymbol{\varepsilon}^{\mathrm{m}}$) and alternating strain tensor ($\boldsymbol{\varepsilon}^{\mathrm{a}}$), respectively. The first principal strains of the mean and alternating strain tensors (${}^{1}\varepsilon^{\mathrm{m}}$ *and* ${}^{1}\varepsilon^{\mathrm{a}}$) are finally obtained automatically by the postprocessor, and $\boldsymbol{\varepsilon}^{\mathrm{m}}$ and $\boldsymbol{\varepsilon}^{\mathrm{a}}$ are calculated as shown

$$\boldsymbol{\varepsilon}^{\mathrm{m}} = [\varepsilon_{ij}^{\mathrm{m}}] = \left[\frac{\varepsilon_{ij}^{\mathrm{L}} + \varepsilon_{ij}^{\mathrm{U}}}{2}\right] \tag{5}$$

$$\boldsymbol{\varepsilon}^{\mathrm{a}} = [\varepsilon_{ij}^{\mathrm{a}}] = \left[\left|\frac{\varepsilon_{ij}^{\mathrm{L}} - \varepsilon_{ij}^{\mathrm{U}}}{2}\right|\right] \tag{6}$$

where $\varepsilon_{ij}^{\mathrm{L}}$ and $\varepsilon_{ij}^{\mathrm{U}}$ are the logarithmic strain tensor components at the end of the loading and unloading steps respectively, and $i, j = 1, 2, 3$.

For the fatigue strain limit, the conclusion that Goodman criterion is not suitable for the Nitinol was drawn by investigating the effect of mean strain on the Nitinol fatigue behaviour [32]. In this work, the fatigue life limit curve proposed by Pelton [31] for 10^7 loading-unloading cycles corresponding to 10 years of gait is simplified as a line corresponding to the alternating strain amplitude of 0.4% [17]. In addition, a safety factor is defined as follows

$$f = \frac{0.004}{{}^{1}\varepsilon^{\mathrm{a}}} \tag{7}$$

A safety factor $f < 1$ indicates that fatigue failure could occur within 10^7 loading-unloading cycles in the particular region, whereas $f > 1$ indicates that the particular region can withstand 10^7 loading-unloading cycles.

3. Results

In this study, four simulations are conducted to gain a better fundamental understanding of the stent fatigue behaviours corresponding to the four different situations: one model without the atherosclerotic plaque is subjected to the complex boundary condition (Case 1), and the other with the atherosclerotic plaque is respectively subjected to single axial compression (Case 2), the boundary condition that combines axial compression with axial bending (Case 3), and the complex boundary condition (Case 4). The simulation results are described as follows.

3.1. Stent deployment results

The radial displacement contour plots of the models with and without the atherosclerotic plaque after stent deployment are shown in Fig. 9. For the model without the atherosclerotic plaque, as can be seen from the plot, the artery lumen diameter of the stented part is

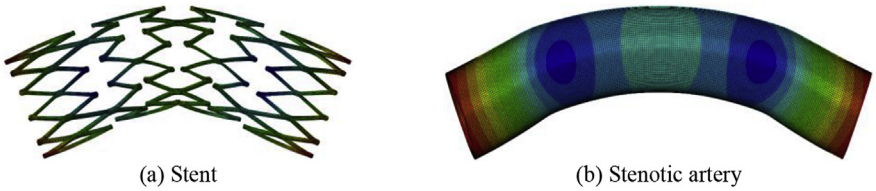

(a) Stent (b) Stenotic artery

Fig. 8. Vibration model corresponding to the fundamental frequency.

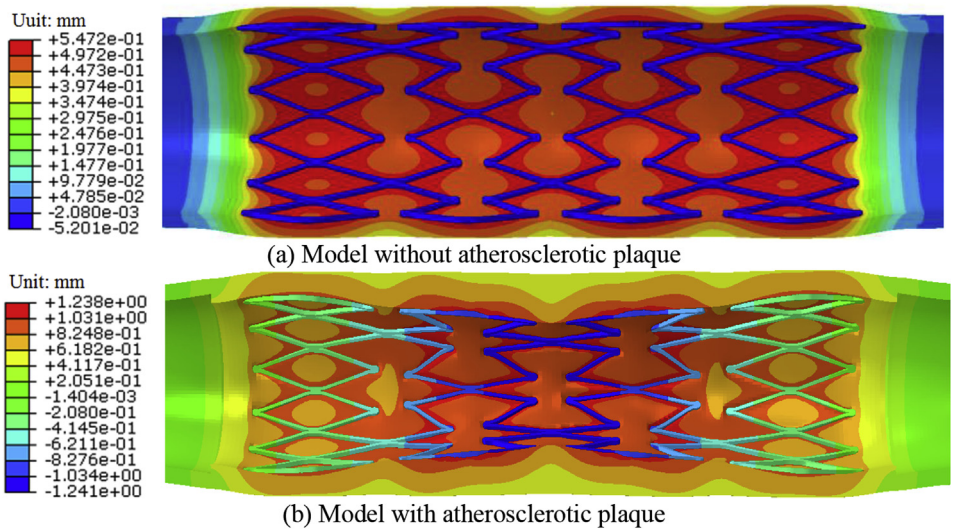

Fig. 9. Radial displacement contour plots of the models after stent deployment.

significantly larger than that of the non-stented portion in the artery model, and no apparent tissue prolapse [22] is observed at the stented site. The entire stent expands evenly in the axial direction, and the stent diameter is decreased by approximately 0.1 mm compared with the initial configuration.

For the model with the atherosclerotic plaque, the implantation of the stent does not completely eliminate stenosis of the diseased artery, and the stenotic artery still has the minimum lumen at the middle site. The minimum inner diameter of the model is 5.16 mm, corresponding to a residual stenosis rate of 26.23%. An obvious tissue prolapse occurs, especially at the middle site of the plaque where the most-narrowing site is located, which decreases the lumen to a great extent. The presence of plaque significantly increases the deformation of the stent, and the stent expansion is extremely non-uniform in the axial direction.

3.2. Stent fatigue behaviours

Cyclic boundary conditions are loaded on the models after stent deployment, and the mean strain contour plots of the stents in the four cases are shown in Fig. 10. In Case 1 (Fig. 10a), overall, the mean strain is distributed relatively evenly along the axial direction of the stent. The strain concentration mainly occurs in the joint between the strut and link, and the maximum value is located in the joint in the middle of the stent. For the stent implanted into the stenotic artery under different boundary conditions (Fig. 10b, c, d), the mean strain distributions are no longer even along the axial direction. The strain concentration still mainly occurs in the joint between the strut and link, but the maximum values are located in the joint at both sides of the plaque peak.

Under the cyclic boundary conditions, the alternating strain contour plots of the stents in the four cases are shown in Fig. 11. In Case 1 (Fig. 11a), the alternating strain is apparently distributed unevenly along the axial direction of the stent, which is inconsistent with the mean strain distribution. The strain concentration mainly occurs in the joint between the strut and link, and the maximum alternating strain is located in the joint between the strut and link in the middle of the stent. The maximum value is 0.10%, corresponding to a safety factor of 4.0, indicating that the stent is absolutely safe in this case.

For the stents implanted into the stenotic artery under different boundary conditions (Fig. 11b, c, d), similar to the mean strain, the alternating strain distributions are also uneven along the axial direction, the strain concentration still mainly occurs in the joint between the strut and link, and the maximum values are located in the joint at both sides of the plaque peak. In Case 2 (Fig. 11b), the maximum alternating strain increases significantly compared with that in Case 1. The maximum value is 0.31%, corresponding to a minimum safety factor of 1.29, thus the stent is safe in this situation. In Case 3 (Fig. 11c), the maximum alternating strain increases significantly compared with that in Case 2. The maximum alternating strain is 0.61%, corresponding to a minimum safety factor of 0.66, which indicates that the stent cannot withstand 10^7 loading-unloading cycles. In this case, cracks will gradually appear and grow in the strain concentration areas, and fatigue failure will eventually occur during the use of the stent. In Case 4 (Fig. 11d), the maximum alternating strain increases slightly compared with that in Case 2. In this case, the minimum safety factor is 0.62, i.e., fatigue fracture will also occur during the use of the stent in the same way.

In addition, scatters ($^1\varepsilon^m$, $^1\varepsilon^a$) of the total 1524,224 Gauss points in the stent in all four cases are drawn for comparison with the 10^7 fatigue life limit curve (Fig. 12). Obviously, large differences occur in the stent fatigue behaviours for the four cases. The stents in both Case 3 and Case 4 are dangerous, and the corresponding unsafe regions are shown more directly in Fig. 13. In conclusion, a summary of the simulation results for all four cases is given in Table 3.

4. Discussion

In this work, to show the necessity and feasibility of considering both physiological deformation and atherosclerotic plaque in the evaluation of stent fatigue behaviours based on FEA, the complete FEA framework is established to simulate the actual stenting procedure, and comparative simulations are successfully conducted for the four different situations. The first principal strains of the mean and alternating strain tensors under the cyclic boundary conditions are respectively regarded as the mean strain and alternating strain to evaluate the Nitinol stent fatigue behaviours by comparison with the simplified 10^7 fatigue life limit curve.

The stent shows two completely different forms when implanted into the normal artery (Fig. 9a) and the stenotic artery (Fig. 9b). The stent in the stenotic artery exhibits a dog-bone shape after deployment [33]. After stent deployment, the maximum residual stenosis rate of the stenotic artery is 26.23%, and thus post-dilatation might be needed [34].

The mean strain is distributed relatively unevenly along the axial direction of the stent in the stenotic artery (Fig. 10b, c, d) compared with the normal artery (Fig. 10a), and the maximum mean strain values of the stent implanted into the stenotic artery are significantly larger than that of the stent implanted into the normal artery. However, under the three different boundary conditions (Fig. 10b, c, d), the mean strain

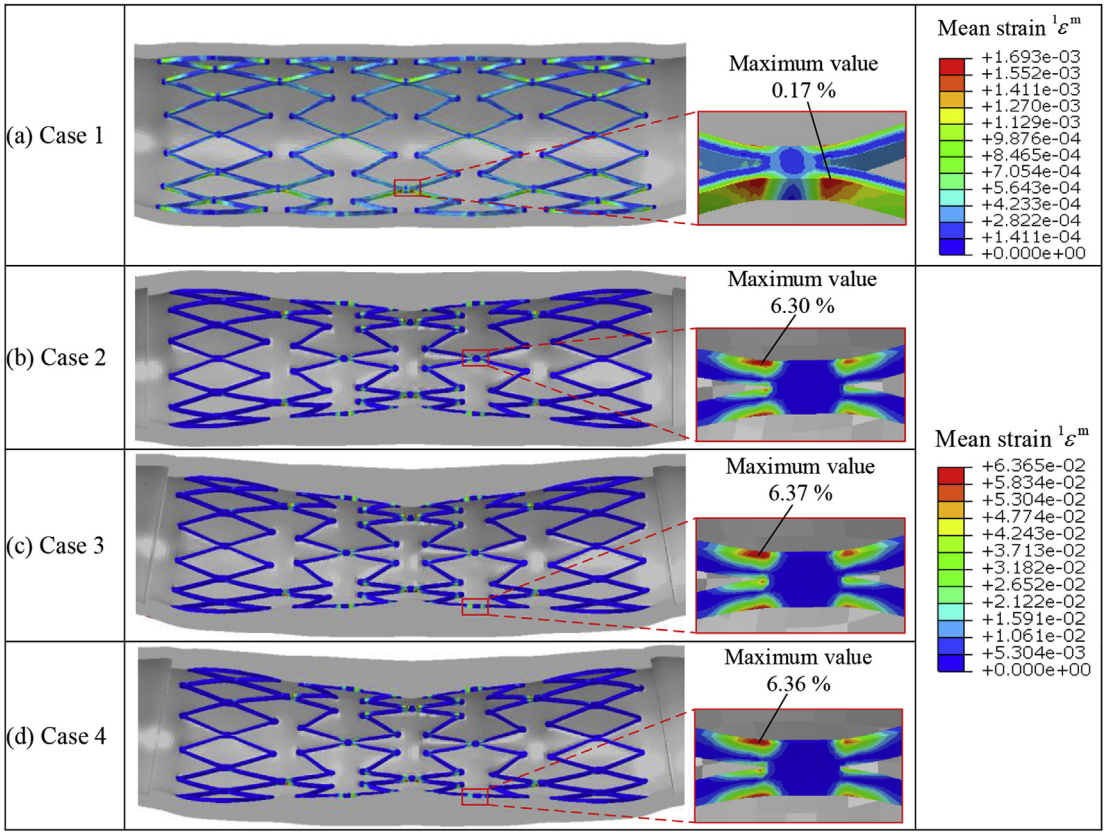

Fig. 10. Mean strain contour plots of the stents in four cases: (a) Case 1 - model without atherosclerotic plaque is subjected to the complex boundary condition; (b) Case 2 - model with atherosclerotic plaque is subjected to single axial compression; (c) Case 3 - model with atherosclerotic plaque is subjected to the boundary condition that combines axial compression with axial bending; (d) Case 4 - model with atherosclerotic plaque is subjected to the complex boundary condition.

distributions are similar, and the maximum mean strain values are almost equal for the stent implanted into the stenotic artery. This result indicates that the atherosclerotic plaque imposes a significantly impact on both the distribution and maximum value of the mean strain, which corroborates the argument that the mean strain is mainly determined by oversizing [11]. Thus, it is necessary to consider the atherosclerotic plaque in stent fatigue life analysis.

The alternating strain distributions along the axial direction of the stent in the stenotic artery (Fig. 11b, c, d) are similar but different from the distribution in the normal artery (Fig. 11a), which implies that the alternating strain distribution is also mainly determined by the atherosclerotic plaque. The maximum alternating strain values lie on both sides of the plaque peak in the presence of plaque, because the area with a smaller lumen has a larger stiffness [11]. It is noteworthy that the maximum alternating strain value of stent in the stenotic artery significantly increases with the superposition of axial bending on axial compression (Fig. 11b and c; Fig. 12b). The maximum alternating strain value in Case 4 is slightly larger than that in Case 3 (Fig. 11c and d; Fig. 12b; Table 3), which is probably due to the small twisting considered. Even so, the stent fatigue fracture is more likely to occur under the complex boundary condition based on the obvious increase in the number of dangerous points in Case 4 compared with Case 3 (Table 3). This result indicates that the deformation boundary condition contributes to the alternating strain value, as also verified by Harley [17]. Based on the fatigue criterion and the simplified fatigue life limit curve, the case that considers the complex boundary condition and atherosclerotic plaque is the most critical of the four cases. In conclusion, the necessity of considering both physiological deformation and atherosclerotic plaque in evaluation of the stent fatigue behaviours based on FEA is confirmed. In other words, the FEA-based simulations in the literature [11,17] overestimated the stent fatigue life, so did *in vitro* tests in the literature [6,9]. Considering the significant adverse effect of atherosclerotic plaque on the stent life, percutaneous transluminal angioplasty before stenting [35] is suggested for treating the lesions in SFA and PA, and atherectomy before stenting [36,37] may be a new choice. For patients, large limb flexion movements such as climbing stairs should be avoided in their daily activities to prevent the stent from undergoing large complex deformation.

In addition, the strain concentration mainly occurs in the joint between the struts and links in all cases, which indicates that the strain concentration site has little to do with the atherosclerotic plaque and deformation boundary condition, and the stent strain concentration could be improved by taping its strut width [38]. An interesting phenomenon is observed that the maximum mean strain is located in the area far away from the centre of the curvature when the stent is bent (Fig. 10a, c, d), while the maximum alternating strain is located in the area near the centre of the curvature (Fig. 11a, c, d). In other words, fatigue crack initiation is more likely to occur in the joint between the strut and the link near the centre of the curvature than in the joint away from the centre of the curvature.

Of course, several limitations exist in this work. In particular, the realistic diseased artery geometry significantly influences the stent fatigue life [39], and the actual artery distinctly consists of the tunica intima, tunica media and tunica adventitia [40,41] and shows different properties in the circumferential and axial directions [42]. However, the idealized stenotic artery model with isotropic material properties is used in this work. In addition, the Nitinol properties highly depend on the applied manufacturing conditions [43,44], but the material property [12] and the fatigue life limit curve [28] are not obtained from the actual stent due to the lack of experimental equipment. These simplifications in the geometry and material properties of the artery, plaque and stent might yield some variance to the predicted fatigue life of the

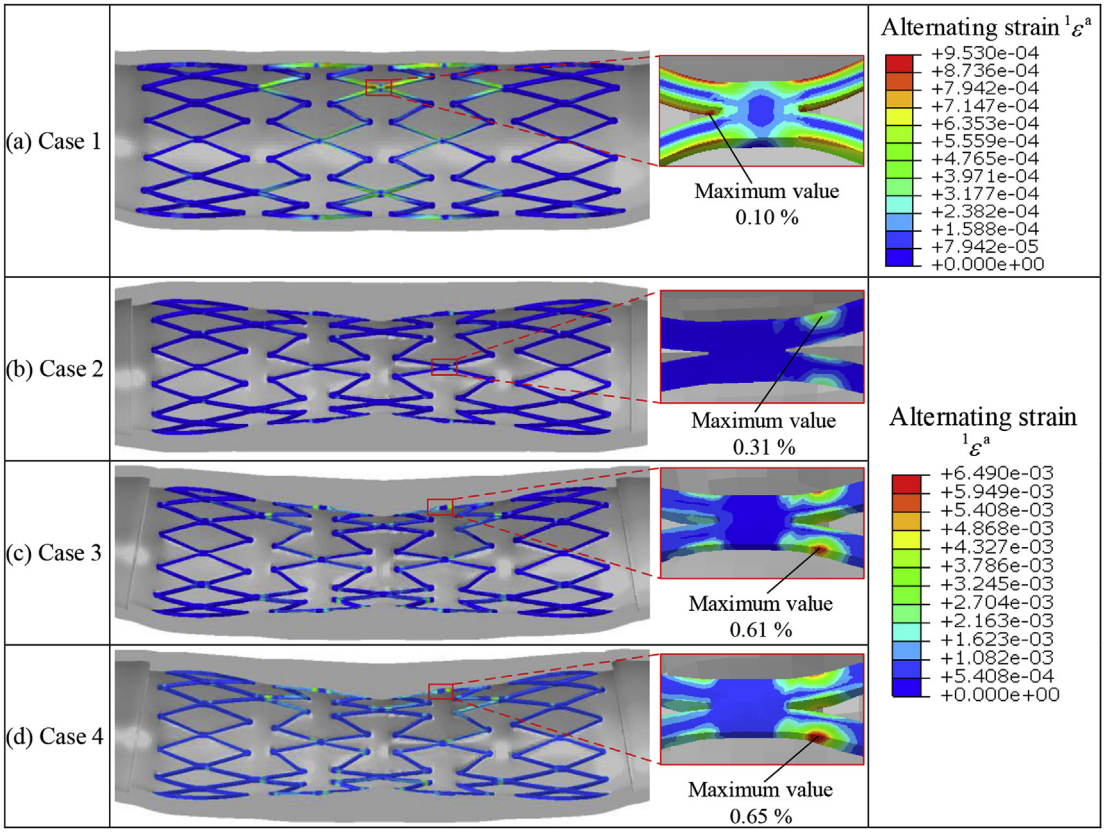

Fig. 11. Alternating strain contour plots of the stents in four cases: (a) Case 1 - model without atherosclerotic plaque is subjected to the complex boundary condition; (b) Case 2 - model with atherosclerotic plaque is subjected to single axial compression; (c) Case 3 - model with atherosclerotic plaque is subjected to the boundary condition that combines axial compression with axial bending; (d) Case 4 - model with atherosclerotic plaque is subjected to the complex boundary condition.

stent, however, the conclusions are reasonable considering the comparative nature of this work. Specifically, the influence of the deformation boundary condition and atherosclerotic plaque on the stent fatigue performance is studied by comparing the distributions and the maximum values of the mean and alternating strains in the four cases. In addition, some conclusions of this work are consistent with those of the literature [11,17]. Additionally, in this study, cyclic pulsatile blood pressure is not considered, the effect of pre-stretching of the stenotic artery on the simulation results remains to be further explored, the fatigue criterion is relatively simple and the multiaxial criterion [17] may be needed. In particular, the results of this paper should be further verified by *in vitro* tests and related to actual patient adverse events [45].

5. Conclusion

Despite certain limitations, the following conclusions can be drawn based on the above simulation results and discussion. It is necessary to consider both physiological deformation and atherosclerotic plaque in evaluation of the stent fatigue behaviours, and ignoring any of them can lead to overestimation of the stent fatigue life. The atherosclerotic plaque contributes to the distribution and maximum value of the mean strain and also to the distribution and maximum value of the alternating strain. The effect of the deformation boundary condition on the stent durability is mainly reflected in the alternating strain value. In addition, the strain concentration site has little to do with the atherosclerotic plaque and deformation boundary condition.

Based on the conclusions and experience in this paper, a more accurate evaluation framework of the stent fatigue lifetime can be established based on FEA in future work. Specifically, all of the

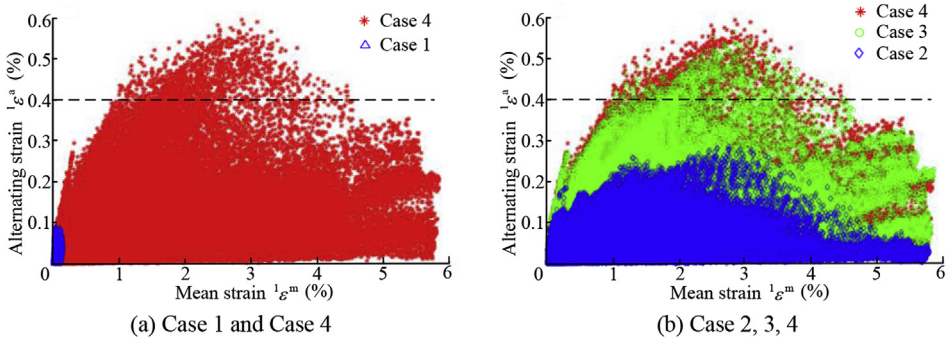

Fig. 12. Scatters ($^1\varepsilon^m$, $^1\varepsilon^a$) of the total 1524,224 Gauss points in the stent in all four cases.

(a) Case 3 (b) Case 4

Fig. 13. Unsafe regions (marked in red) of the stents in Case 3 and Case 4.

Table 3
Summary of the simulation results from four perspectives for all four cases.

Indicators	Case 1	Case 2	Case 3	Case 4
Maximum mean strain (%)	0.17	6.30	6.37	6.36
Maximum alternating strain (%)	0.10	0.31	0.61	0.65
Minimum safety factor	4.0	1.29	0.66	0.62
No. of dangerous Gauss points	0	0	809	1137

limitations should be properly addressed. For example, the diseased artery model will be generated from CT angiography scans of actual PAD patients and the whole stent model obtained from the DICOM images based on 3D reconstruction will be used directly.

Conflicts of interest

None Declared.

Acknowledgements

This work was supported by the Shenzhen Fundamental Research Funds (Grant No. JCYJ20160608153218487) and the National Key R& D Program of China (Grant No. 2017YFC0110600), in part by the Shenzhen Key Laboratory Project (Grant No. ZDSYS201707271637577), the National Natural Science Foundation of China (Grant Nos. U1613224, U1713218), and the Shenzhen Peacock Plan (Grant No. KQTD2016113010571019).

References

[1] GBD 2015 Mortality and Causes of Death, Collaborators. Global, regional, and national life expectancy, all-cause mortality, and cause-specific mortality for 249 causes of death, 1980–2015: a systematic analysis for the Global Burden of Disease Study 2015, Lancet 388 (10053) (2016) 1459–1544.
[2] GBD 2015 Disease and Injury Incidence and Prevalence, Collaborators. Global, regional, and national incidence, prevalence, and years lived with disability for 310 diseases and injuries, 1990-2015: a systematic analysis for the Global Burden of Disease Study 2015, Lancet 388 (10053) (2016) 1545–1602.
[3] A. Fortier, V. Gullapalli, R.A. Mirshams, Mirshams. Review of biomechanical studies of arteries and their effect on stent performance, IJC Heart & Vessels 4 (2014) 12–18.
[4] L. Petrini, F. Migliavacca, P. Massarotti, S. Schievano, G. Dubini, F. Auricchio, Computational studies of shape memory alloy behavior in biomedical applications, J. Biomech. Eng. 127 (4) (2005) 716–725.
[5] J. Rits, J.A. Van Herwaarden, A.K. Jahrome, D. Krievins, F.L. Moll, The incidence of arterial stent fractures with exclusion of coronary, aortic, and non-arterial settings, Eur. J. Vasc. Endovasc. Surg. 36 (3) (2008) 339–345.
[6] S. Müller-Hülsbeck, P.J. Schäfer, N. Charalambous, H. Yagi, M. Heller, T. Jahnke, Comparison of second-generation stents for application in the superficial femoral artery: an in vitro evaluation focusing on stent design, J. Endovasc. Ther. 17 (6) (2010) 767–776.
[7] K. Maleckis, P. Deegan, W. Poulson, C. Sievers, A. Desyatova, J. MacTaggart, A. Kamenskiy, Comparison of femoropopliteal artery stents under axial and radial compression, axial tension, bending, and torsion deformations, J. Mech. Beh. Biomed. Mat. 75 (2017) 160–168.
[8] W. Xue, J. Gao, J. Lin, F. Wang, G. Guan, L. Wang, Deformation mechanisms of prototype composite braided stent-grafts in bending fatigue for peripheral artery application, J. Mech. Beh. Biomed. Mat. 78 (2018) 74–81.
[9] A. Nikanorov, H.B. Smouse, K. Osman, M. Bialas, S. Shrivastava, L.B. Schwartz, Fracture of self-expanding nitinol stents stressed in vitro under simulated intravascular conditions, J. Vasc. Surg. 48 (2) (2008) 435–440.
[10] M. Early, D.J. Kelly, The consequences of the mechanical environment of peripheral arteries for nitinol stenting, Med. Biol. Eng. Comput. 49 (11) (2011) 1279–1288.
[11] E. Dordoni, A. Meoli, W. Wu, G. Dubini, F. Migliavacca, G. Pennati, L. Petrini, Fatigue behaviour of Nitinol peripheral stents: the role of plaque shape studied with computational structural analyses, Med. Eng. Phys. 36 (7) (2014) 842–849.
[12] A. Meoli, E. Dordoni, L. Petrini, F. Migliavacca, G. Dubini, G. Pennati, Computational modelling of in vitro set-ups for peripheral self-expanding nitinol stents: the importance of stent–wall interaction in the assessment of the fatigue resistance, Cardiovascular Engineering and Technology 4 (4) (2013) 474–484.
[13] L. Petrini, W. Wu, E. Dordoni, A. Meoli, F. Migliavacca, G. Pennati, Fatigue behavior characterization of nitinol for peripheral stents, Funct. Mat. Lett. 5 (01) (2012) 1250012.
[14] A. Meoli, E. Dordoni, L. Petrini, F. Migliavacca, G. Dubini, G. Pennati, Computational study of axial fatigue for peripheral nitinol stents, J. Mater. Eng. Perform. 23 (7) (2014) 2606–2613.
[15] E. Dordoni, L. Petrini, W. Wu, F. Migliavacca, G. Dubini, G. Pennati, Computational modeling to predict fatigue behavior of NiTi stents: what do we need? J. Funct. Biomater. 6 (2) (2015) 299–317.
[16] L. Petrini, A. Trotta, E. Dordoni, F. Migliavacca, G. Dubini, P.V. Lawford, et al., A computational approach for the prediction of fatigue behaviour in peripheral stents: application to a clinical case, Ann. Biomed. Eng. 44 (2) (2016) 536–547.
[17] S.M. Harvey, Nitinol stent fatigue in a peripheral human artery subjected to pulsatile and articulation loading, J. Mater. Eng. Perform. 20 (4–5) (2011) 697–705.
[18] R.N. Ghriallais, M. Bruzzi, A computational analysis of the deformation of the femoropopliteal artery with stenting, J. Biomech. Eng. 136 (7) (2014) 071003.
[19] B.M. Learoyd, M.G. Taylor, Alterations with age in the viscoelastic properties of human arterial walls, Circ. Res. 18 (3) (1966) 278–292.
[20] S. Pant, N.W. Bressloff, G. Limbert, Geometry parameterization and multidisciplinary constrained optimization of coronary stents, Biomechanics Model. Mechanobiol. 11 (1–2) (2012) 61–82.
[21] R.M. Hicks, P.A. Henne, Wing design by numerical optimization, J. Aircraft 15 (7) (2012) 407–412.
[22] S. Zhao, L. Gu, S.R. Froemming, Performance of self-expanding Nitinol stent in a curved artery: impact of stent length and deployment orientation, J. Biomech. Eng. 134 (7) (2012) 071007.
[23] D. Gastaldi, S. Morlacchi, R. Nichetti, C. Capelli, G. Dubini, L. Petrini, F. Migliavacca, Modelling of the provisional side-branch stenting approach for the treatment of atherosclerotic coronary bifurcations: effects of stent positioning, Biomechanics Model. Mechanobiol. 9 (5) (2010) 551–561.
[24] C. Conway, F. Sharif, J.P. McGarry, P.E. McHugh, A computational test-bed to assess coronary stent implantation mechanics using a population-specific approach, Cardiovascular Engineering and Technology 3 (4) (2012) 374–387.
[25] E.M. Cunnane, J.J. Mulvihill, H.E. Barrett, M.T. Walsh, Simulation of human atherosclerotic femoral plaque tissue: the influence of plaque material model on numerical results, Biomed. Eng. Online 14 (1) (2015) 1–12.
[26] F. Auricchio, R.L. Taylor, J. Lubliner, Shape-memory alloys: macromodelling and numerical simulations of the superelastic behavior, Comput. Methods Appl. Mech. Eng. 146 (3) (1997) 281–312.
[27] A.J. Klein, S. James Chen, J.C. Messenger, A.R. Hansgen, M.E. Plomondon, J.D. Carroll, I.P. Casserly, Quantitative assessment of the conformational change in the femoropopliteal artery with leg movement, Cathet. Cardiovasc. Interv. 74 (5) (2009) 787–798.
[28] A. Ganguly, J. Simons, A. Schneider, B. Keck, N.R. Bennett, R.J. Herfkens, et al., In-vivo imaging of femoral artery nitinol stents for deformation analysis, J. Vasc. Intervent. Radiol. 22 (2) (2011) 244–249.
[29] J.N. MacTaggart, N.Y. Phillips, C.S. Lomneth, I.I. Pipinos, R. Bowen, B.T. Baxter, et al., Three-dimensional bending, torsion and axial compression of the femoropopliteal artery during limb flexion, J. Biomech. 47 (10) (2014) 2249–2256.
[30] F. Ansari, L.K. Pack, S.S. Brooks, T.M. Morrison, Design considerations for studies of the biomechanical environment of the femoropopliteal arteries, J. Vasc. Surg. 58 (3) (2013) 804–813.
[31] A.R. Pelton, Nitinol fatigue: a review of microstructures and mechanisms, J. Mater. Eng. Perform. 20 (4–5) (2011) 613–617 2011. 20(4): p. 613 - 617.
[32] R.M. Tabanli, N.K. Simha, B.T. Berg, Mean stress effects on fatigue of NiTi, Mater. Sci. Eng. 273 (1999) 644–648.
[33] S. Zhao, L. Gu, S.R. Froemming, Assessment of shape memory alloy stent deployment in a stenosed artery, Biomed. Eng. Lett. 1 (4) (2011) 226–231.
[34] E. Romagnoli, G.M. Sangiorgi, J. Cosgrave, E. Guillet, A. Colombo, Drug-Eluting Stenting: the case for post-dilation, JACC Cardiovasc. Interv. 1 (1) (2008) 22–31.
[35] J.R. Laird, B.T. Katzen, D. Scheinert, J. Lammer, J. Carpenter, M. Buchbinder, et al., Nitinol stent implantation versus balloon angioplasty for lesions in the superficial femoral artery and proximal popliteal artery: twelve-month results from the RESILIENT randomized trial, Circulation: Cardiovascular Interventions 109 (2010) 903468 CIRCINTERVENTIONS.
[36] G.K. Ambler, R. Radwan, P.D. Hayes, C.P. Twine, Atherectomy for peripheral arterial disease, Cochrane Database Syst. Rev. (3) (2014).
[37] I. Moussa, C. Di Mario, J. Moses, B. Reimers, L. Di Francesco, G. Martini, et al., Coronary stenting after rotational atherectomy in calcified and complex lesions: angiographic and clinical follow-up results, Circulation 96 (1) (1997) 128–136.
[38] H.M. Hsiao, L.W. Wu, M.T. Yin, C.H. Lin, H. Chen, Quintupling fatigue resistance of intravascular stents via a simple design concept, Comput. Mater. Sci. 86 (2014) 57–63.
[39] X. Cui, Q. Ren, G. Li, Z. Li, A. Qiao, Influence of the realistic artery geometry

parameters on a coronary stent fatigue life, Int. J. Comput. Methods (2018) 1842006.
[40] G. Sommer, Mechanical Properties of Healthy and Diseased Human Arteries, TU Graz, 2008.
[41] C. Conway, J.P. McGarry, E.R. Edelman, P.E. McHugh, Numerical simulation of stent angioplasty with predilation: an investigation into lesion constitutive representation and calcification influence, Ann. Biomed. Eng. 45 (9) (2017) 2244–2252.
[42] W.W. von Maltzahn, R.G. Warriyar, W.F. Keitzer, Experimental measurements of elastic properties of media and adventitia of bovine carotid arteries, J. Biomech. 17 (11) (1984) 839–847.
[43] A.R. Pelton, V. Schroeder, M.R. Mitchell, X.Y. Gong, M. Barney, S.W. Robertson, Fatigue and durability of Nitinol stents, Journal of the mechanical behavior of biomedical materials 1 (2) (2008) 153–164.
[44] S.W. Robertson, A.R. Pelton, R.O. Ritchie, Mechanical fatigue and fracture of Nitinol, Int. Mater. Rev. 57 (1) (2012) 1–37.
[45] K.D. Everett, C. Conway, G.J. Desany, B.L. Baker, G. Choi, C.A. Taylor, E.R. Edelman, Structural mechanics predictions relating to clinical coronary stent fracture in a 5 year period in FDA MAUDE database, Ann. Biomed. Eng. 44 (2) (2016) 391–403.

Long Lei received the B.S. degree from Harbin University of Science and Technology, Harbin, China, in 2014, and the M.S. degree from Harbin Institute of Technology (Shenzhen), Shenzhen, China, in 2017. He is currently a Ph.D. student in Harbin Institute of Technology (Shenzhen). His research interests include surgical robot, medical image processing, and biomechanics.

Xiaozhi Qi received a B.S. degree from Yanshan University, in 2009, and M.S. and Ph.D. degrees from Harbin Institute of Technology (Shenzhen), China, in 2011 and 2017, respectively. He is currently a postdoctor at the Centre for Cognitive Technology, Shenzhen Institute of Advanced Technology, Chinese Academy of Sciences, China. His current research interests include medical assistant robots and space deployable mechanisms.

Shibo Li received the B.S. and M.S. degrees in aerospace engineering from Beihang University, Beijing, China, in 2009 and 2012, respectively, and Ph.D. degree in engineering mechanics from the University of Alabama, Tuscaloosa, AL, US. He is currently a postdoctoral research assistant in Shenzhen Institute of Advanced Technology, Chinese Academy of Sciences, China. His research interests include biomechanics, computational mechanics and multiscale modelling.

Yuanyuan Yang received the B.S. and Ph.D. degrees in instrument science and technology from Harbin Institute of Technology, Harbin, China, in 2009 and 2017, respectively. He is currently a postdoctoral research assistant in Shenzhen Institute of Advanced Technology, Chinese Academy of Sciences, China. His research interests include computational mechanics, computer assisted surgery and surgical robot.

Ying Hu received the B.S. degree from Shanghai Jiaotong University, Shanghai, China, in 1991, and the M.S. and Ph.D. degrees in mechanical engineering from Harbin Institute of Technology, Shenzhen, China, in 1998 and 2007, respectively. She is currently a Professor Shenzhen Institute of Advanced Technology, Chinese Academy of Sciences, China. She is the author or coauthor of more than 60 scientific papers published in refereed journals and conference proceedings. Her research interests include parallel robots, medical assistant robots, and mobile robots.

Bing Li received the Ph.D. degree from Hong Kong Polytechnic University, Hong Kong, in 2001. He was a Professor of Mechatronics in 2006. He is currently the Head of the School of Mechanical Engineering and Automation with the Harbin Institute of Technology (Shenzhen), China. His research interests include parallel manipulators, mechanical vibration and control. Prof. Li is serving as an Associate Editor of the International Journal of Mechanisms and Robotic Systems.

Shijia Zhao received the B.S. and M.S. degrees in Mechanical Engineering from Sichuan University, China in 2003 and 2009, respectively, and Ph.D. degree in Mechanical Engineering & Applied Mechanics from the University of Nebraska-Lincoln, US. He is currently a postdoctoral research fellow in University of Nebraska Medical Centre, Omaha, US. His research interests include medical imaging, biomechanics and computational mechanics.

Yanfang Zhang received the M.S. degree in interventional Radiology from Tongji Medcal University, Wuhan, China. In 1994, and Ph.D. degree in Interventional Radiology from Tongji Medcal College, Huazhong University of Sciencise and Technology, Wuhan, China. In 2002. And He was a Visiting Scholar Majoring in Interventional Radiology and Imaging Diagnostics in Bremerhaven Hospital of GÖttingen University in Germany in 2005. He is currently a Chief Physician in Shenzhen People's Hospital, the Second Affiliated Hospital of Jinan University, Shenzhen, China. His focusing research on vascular intervention (including peripheral vascular intervention. abdominal aortic aneurysm EVAR. And renal artery intervention) and tumor intervention.